Effect of hydrostatic pressure on optical absorption spectrum AlGaN/GaN multi-quantum well

Scientific research paper

Rajab Yahyazadeh[*], Zahra Hashempour

Department of Physics, Islamic Azad University, Khoy branch, Khoy, Iran

ABSTRACT

The current paper investigates the optical absorption spectrum of $Al_{0.3}Ga_{0.7}N/$ GaN multi-quantum well (MQW) under hydrostatic pressure. To obtain the parameters of $Al_{0.3}Ga_{0.7}N/GaN$ MQW, such as electron and hole density, bandgap, interband transition energy, electron-hole wave functions, effective mass and dielectric constant, and the hydrostatic pressure effects are taken into account. Finite difference techniques have been used to acquire energy eigenvalues and their corresponding eigenfunctions of $Al_{0.3}Ga_{0.7}N/GaN$ MQW and the hole eigenstates are calculated via a 6×6 k.p method under an applied hydrostatic pressure. It was found that the depth of the quantum wells, bandgaps, band offset, the electron, and hole density increases with the hydrostatic pressure. Also, as the pressure increases, the electron and hole wave functions will have less overlap, the amplitude of the absorption coefficient increases, and the binding energy of the excitons decreases. A change in pressure of up to 10 GPa causes the absorption coefficients peaks of light and heavy holes to shift to low wavelengths of up to 32 nm.

1 Introduction

Nitride heterostructures are important because of the high energy gap, the high electron density in the quantum well, and the high electrical conductivity [1,2]. These heterostructures are used in the manufacture of electronic components (e.g. transistors and diodes, optical components, solar cells) and industrial components such as electrical switches (disconnecting or connecting electrical circuits that act as converters) [3-4]. The binding energy of AlGaN/GaN excitons and

other optical behaviors may vary under the influence of external perturbations, such as temperature, magnetic field, and pressure [5,6]. Therefore, it is important to study the effect of hydrostatic pressure on optical parameters such as the absorption coefficient. Given that the absorption coefficient is the most important parameter in calculating and studying the current in solar cells, it needs to be studied under external pressure perturbations. Bardyszewski et al. examined the binding energy of excitons under hydrostatic pressure [7]. Asgari et al. [8] calculated the adsorption coefficient for InGaN / GaN MQW at different impurities and different

well widths. Stevens et al. [9] calculated the absorption coefficient of AlGaAs/GaAs MQW. Most articles present the analytical formula obtained from the experimental results for the absorption coefficient, which depends on the energy gap used in the calculation of the photoelectric current of solar cells. A precise measure of the absorption coefficient also requires numerical calculations. [10]. Therefore, in this paper, we study the behavior of the adsorption coefficient of AlGaN / GaN multiple quantum wells under external pressure (external disturbance), which has not been done numerically. The most important advantages of this numerical method and the aspect of innovation in this work are based on five important parameters: effective mass, energy gap, lattice constants, dielectric constant and quantum barrier, and well-thickness, which are simultaneously dependent on hydrostatic pressure and temperature. We also considered the effect of hydrostatic pressure on the energy of heavy and light holes and the transition energy of the subbands.

In this model, we obtain the conduction band energy, wave functions, and energy subbands from the self-consistent solution of the Schrodinger and Poisson equations. The hole valance bands (heavy and light hole) energy, wave functions, and energy subbands are calculated using a 6×6 **k.p** method. These calculations consider up to 5 energy subbands in quantum wells. The sample used in the modeling is the p–i–n solar cells with an AlGaN/GaN MQW structure within the i-region. The p and n regions are based on GaN. The donor and acceptor concentrations in the n- and p-region materials are assumed to be the same, where in this study the volume is assumed about $0.1 \times 10^{18} cm^3$ with 25 wells. Only the first subband transition (with uncoupled heavy and light hole states) has been considered in this calculation. The absorption spectrum of the MQW structure has been determined via these transition energy and wave functions. It should be notified that the calculated built in polarization field for the structures is about $\sim 10^8 V/m$. In this work, the atmospheric and hydrostatic pressures are taken into account. That is, at zero hydrostatic pressure, only atmospheric pressure is applied. The results and discussions are obtained by calculating and drawing the figures.

2 Hetrostructure Modeling

2.1 Self-consistent solution of Schrödinger-Poisson equations

The MQW structure introduced for the model is constructed by a AlGaN with bandgap energy of E_{gAlGaN} for the barriers and GaN for the wells, which is schematically shown in Fig. 1. In order to obtain accurate values for Fermi energy, the energies of quantized levels within the 2DEG, potential profiles, wave function, and the sheet carrier concentration for the 2DEG in AlGaN/GaN heterostructures, both the Schrodinger and Poisson equations must be solved self consistently. This has been achieved by solving Schrodinger's equation and simultaneously taking into account the electrostatic potential obtained from the Poisson's equation, as well as the image and exchange-correlation potentials using the three-point finite difference method. The Schrodinger equation in quantum structures is introduced as follows [11]

$$-\frac{\hbar^2}{2}\frac{d}{dz}\left(\frac{1}{m_e^*}\frac{d\psi_n(z)}{dz}\right) + E_c(z)\psi_n(z) = E_n\psi_n(z), \tag{1}$$

where $\hbar$ represents the reduced Planck constant, m_e^* electron effective mass, E_c the total potential function, ψ_n the nth state wave function, with its associated nth state energy level E_n. In total potential ($E_c(z)$), the following expression is included

$$E_c(z) = V_B(z) + V_H(z) + V_{ex}(z) + V_P(z), \tag{2}$$

Where $V_B(z)$ is the heterojunction band gap discontinuity, $V_H(z)$ is the effective Hartree potential, and $V_{ex}(z)$ is the exchange-correlation potential.

2.2 Potential energy of polarization charges

The $V_P(z) = eF_z z$ is the potential energy induced by the polarization charges while F_z is the electric fields in the well (F_w) and barrier (F_b) caused by the spontaneous (SP) and piezoelectric (PZ) polarization given by [12,13]

$$F_w = \frac{\sigma_s(T,P,m)L_b}{\varepsilon_0(\varepsilon_w L_w + \varepsilon_b L_b)}, \tag{3}$$

$$F_b = -\frac{\sigma_s(T,P,m)L_w}{\varepsilon_0(\varepsilon_w L_w + \varepsilon_b L_b)} = -F_w\frac{L_w}{L_b}, \tag{4}$$

where $\sigma_s(T,P,m)$ is total polarization at the interface AlGaN/GaN expressed as [14, 15]

$$\sigma_s(T,P,m) = \left| P^{PZ}_{Al_mGa_{1-m}N} + P^{SP}_{Al_mGa_{1-m}N} - P^{SP}_{GaN} \right.$$
$$\left. - P^{PZ}_{GaN} \right|, \tag{5}$$

where

$$P^{PZ}_{GaN} = -0.918\epsilon + 9.541\epsilon^2, \tag{6}$$

$$P^{PZ}_{AlN} = \begin{cases} -1.808\epsilon + 5.624\epsilon^2 & for\ \epsilon < 0 \\ -1.808\epsilon - 7.888\epsilon^2 & for\ \epsilon > 0 \end{cases}, \tag{7}$$

$$P^{SP}_{Al_mGa_{1-m}} = 0.090m - 0.034(1-m)$$
$$+ 0.21x(1-m). \tag{8}$$

The basal strain is expressed from the lattice of substrate a_s and the epilayer $a_e(T,P,m)$ as

$$\epsilon(T,P,m) = \frac{a_c - a_e(T,P,m)}{a_e(T,P,m)}. \tag{9}$$

The lattice constants, as a function of temperature, alloy and the hydrostatic pressure given by [16, 17]

$$a_e(T,P,m) = a_0(m)\left[\left(1 + \beta\left(T - T_{ref}\right)\right)\left(1 - \frac{P}{3B_0}\right)\right], \tag{10}$$

where $B_0 = 239GPa$ is the bulk modulus of sapphire. $\beta_{GaN} = 5.56 \times 10^{-6}K^{-1}$ is the thermal expansion coefficient and $T_{ref} = 300K^0$. $a_0(m)$, is the equilibrium lattice constant as a function of composition given by [18, 19]

$$a_0(m) = 0.13989m + 0.03862. \tag{11}$$

Here the dielectric constant $(\varepsilon_{GaN}(T,P),$ $\varepsilon_{AlGaN}(m,T,P))$) of the GaN, AlGaN, and AlGaN barrier thickness ($_{Al_mGa_{1-m}N}(\ ,\ )$ as a function of preasure and temperature are given by [5,19,20] as

$$\varepsilon_{GaN}(T,P) = 10$$
$$\times \exp(10^{-4}(T - T_0) - 6.7$$
$$\times 10^{-3}P), \tag{12}$$

$$\varepsilon_{AlGaN}(m,T,P) = \varepsilon^{GaN}(T,P) + 0.03m, \tag{13}$$

$$=\ _{Al_mGa_{1-m}N}(\ ,\ )$$
$$=\ (0)\left[-\left(\ ^{Al_mGa_{1-m}N}_{11}\right.\right.$$
$$\left.\left. + 2\ ^{Al_mGa_{1-m}N}_{12}\right)\right], \tag{14}$$

$$=\ _{GaN}(\ ,\ ) =\ (0)\left[-\left(\ ^{GaN}_{11}\right.\right.$$
$$\left.\left. + 2\ ^{GaN}_{12}\right)\right]. \tag{15}$$

Here, (0) and (0) are the AlGaN and GaN layers thickness without hydrostatic pressure and temperature. $_{11}$, $_{12}$ are the elastic compliance constants of $Al_mGa_{1-m}N$ which are given by [5, 20]

$$_{11} = \frac{_{11}\ _{33} -\ ^2_{13}}{(\ _{11} -\ _{12})[\ _{33}(\ _{11} +\ _{12}) - 2\ ^2_{13}]}. \tag{16}$$

$$_{12} = \frac{_{12}\ _{33} -\ ^2_{13}}{(\ _{11} -\ _{12})[\ _{33}(\ _{11} +\ _{12}) - 2\ ^2_{13}]}. \tag{17}$$

2.2 Effective Hartree potential

The effective Hartree potential describes the electrostatic interaction of electrons with themselves and with ionized impurities. This is obtained by solving the following Poisson equation:

$$\frac{d^2V_H(z,P,T)}{dz^2} = \frac{e^2}{\varepsilon_0\varepsilon_{GaN(P,T)}}(N_D(z) - n_{2D}(z,P,T)), \tag{18}$$

where n_{2D} represents the electron density of the confined electrons, and N_D is the total doping concentration. The sheet density in the quantum well is given as

$$n_{2D}(z) = \sum_{i=1}^{5} \frac{m^*K_BT}{\pi\hbar^2}ln\left[1 + \exp(\frac{E_F - E_i}{K_BT}\right]\psi_i^2(z), \tag{19}$$

where K_B is the Boltzmann constant, E_F denotes the Fermi level, i represents the subband level index, and T is the absolute temperature. In the numerical model $\Delta d_{2DEG} = 1/n_{2D}\int zn_{2D}(z)dz$ represents the effective width of the 2DEG channel [21].

2.3 Exchange correction potential

The exchange correction potential is evaluated as [22]

$$
V_{ex}(z) = -0.985 \frac{e^2}{4\pi\varepsilon_0\varepsilon_{GaN}(T,P)} n_{2D}^{\frac{1}{3}}(z) \left\{ 1 \right.
$$
$$
+ \frac{0.034}{a_H^* n_{2D}^{\frac{1}{3}}(z)} \ln\left[1 \right.
$$
$$
\left. + 18.376 a_H^* n_{2D}^{\frac{1}{3}}(z) \right] \right\}. \tag{20}
$$

Here, the radius Bohr is obtained by $a_H^* = 4\pi\varepsilon_0\varepsilon_{GaN}\hbar^2/m_e^* e^2$.

2.4 The conduction band offset energy

The conduction band offset energy ΔE_c of AlGaN/GaN hetro interface is obtained as follows [14]

$$
\Delta E_c(P,T) = 0.75\left[E_g^{AlGaN}(P,T) - E_g^{GaN}(P,T)\right], \tag{21}
$$

while $E_g^{AlGaN}(P,T)$ is the band gap variation as a function of the pressure and temperature of AlGaN given by

$$
E_g^{AlGaN}(P,T) = xE_g^{AlN}(P,T) + (1-x)E_g^{GaN}(P,T) - x(1-x), \tag{22}
$$

where $E_g^{AlGaN}(P,T)$ is the band gap from $E_g^{AlN}(P,T)$ and $E_g^{GaN}(P,T)$ respectively, obtained as follows [23]

$$
E_g(T,P) = E_g(0,0) + \gamma P + \sigma P^2 + \frac{\alpha T^2}{T + T_e}. \tag{23}
$$

It is worth noting that $E_g(0,0)$ represents the band gap energy of GaN or AlGaN in the absence of the hydrostatic pressure and at a temperature of 0K. The suggested parameters used in Eq. (20) in our calculations have been taken from Ref 20.

2.5 Electron effective mass

In the Schrödinger equation the electron effective mass m^* can be written as [21]

$$
\frac{m_0}{m_e^*(P,T,m)} = 1
$$
$$
+ \frac{E_P^\Gamma \left(E_g^\Gamma(P,T,m) + 2\Delta_{S0}/3\right)}{E_g^\Gamma \left(E_g^\Gamma(P,T,m) + \Delta_{S0}\right)}, \tag{24}
$$

where m_0 is the free electron mass, E_P^Γ is the energy linked to the momentum matrix element, Δ_{S0} is the spin-orbit splitting, and $E_g^\Gamma(P,T,m)$ is the band gap variation as a function of the hydrostatic pressure and temperature.

2.6 Hole Wave functions and energy subbands

The hole wave functions and energy subbands are calculated along the Z axis using a 6×6 **k.p** method [24]. The hole distribution is calculated by summing the contributions from 5 hole subbands. A formulation is used to calculate the hole distribution as follows [25]

$$
P_{2D}(z) = \frac{m_h^* K_B T}{\pi\hbar^2} \sum_{i=1}^{5} \sum_{v}^{3} |g_i^v(z)| \ln\left[1 \right.
$$
$$
\left. + \exp(\frac{E_i - E_F}{K_B T}\right], \tag{25}
$$

in which m_h^* is an average hole mass in the $k_x - k_y$ plane, E_i is the hole wave functions, $g_i^v(z)$ is the envelope function associated with the n-th basis state of the Hamiltonian, The summation over n is over the three basis state while the summation over j is over the hole wave function. The envelope functions are normalized such that

$$
\sum_{v=1}^{3} \int_0^{L_{GaN}} |g_i^v(z)|^2 dz = 1. \tag{26}
$$

2.7 Absorption spectrum

The optical absorption spectrum of multiple quantum well material in an electric field can be written as [9]

$$
\alpha(\hbar\omega, F)
$$
$$
= M_{cv}^2(F).q_{ex}.L\left(\hbar\omega, E_{CV}^{1,1}(F) - E_b\right)
$$
$$
+ \int_{E_{CV}^{1,1}(F)}^{\infty} M_{cv}^2(F).Nq_{com}.K\left(E', E_{cv}^{1,1}(F)\right)
$$
$$
L(\hbar\omega, E')dE', \tag{27}
$$

where the Lorentzian function is defined as

$$L(\hbar\omega, E)$$
$$= \frac{\Gamma^2_{hom}}{2\pi[(\hbar\omega - E)^2 + \Gamma^2_{hom}]}, \qquad (28)$$

where $\hbar\omega$ is the photon energy, $E_{cv}^{1,1}(F)$ is the separation between the n = 1 valence and conduction subbands, E_b is the exaction binding energy, Γ_{hom} is the full width at half maximum (FWHM) of the homogeneous broadening caused by phonon interaction and tunneling through barriers, q_{ex}. and q_{com} are the oscillator strengths of the excitonic and band to band transitions, respectively, N is the joint density of states between valence and conduction bands while K is continuum shape of the Sommerfeld factor[9]. The electron–hole overlap integral is defined as

$$M_{cv,P} = |\int \psi_{c.P}^*(x)\psi_{v.P}(x)dx|. \qquad (29)$$

It should be mentioned that the assumption of Elliot's theory regarding the absorption used in this manuscript are: (i) a continuum of transitions between free particle states and (ii) excitonic transitions. Also, in excitonic transition, only the first exciton state (1S) is considered. The electric field (F) inside the generic jth layer (either QW or barrier) is given by Eqs. (3) and (4). The ratio of the exciton area to the level of the continuum is given by $q_{ex}/Nq_{com} = 12R_y$, where R, is the Rydberg constant.

3 Results and Discussion

In this paper, we presented a numerical model to calculate the optical absorption spectrum in $Al_{0.3}Ga_{0.7}N/GaN$ multi-quantum wells, which investigate the effect of the hydrostatic pressure. We conducted the iteration between the Schrödinger–Poisson equation systems by a three-point finite difference method to obtain a self-consistent solution of basic equations. During the self-consistent calculation, a grid spacing as small as $1 \times 10^{-10}m$ and the convergent criteria for the electrostatic potential is set to be 0.1% to ensure the iteration convergence and stability of our calculation. The hole eigenstates are calculated along the Z-axis using a 6×6 **k.p** method. Figure 2 shows the dependence of the conduction band offset, the bandgaps of AlGaN, and GaN to the hydrostatic pressure. The increase in the hydrostatic pressure with a range of 0-10Pa leads to the increase of the conduction band offset. This is attributed to an increase in the bandgap energy of GaN and AlGaN with an HP increase. This phenomenon is related to the correction of the atomic distances of the crystal lattice by external pressure, which also leads to a change in polarization. The insert of Figure 2 shows the variations in the σ_b versus the hydrostatic pressure. As the pressure increases, σ_b rises due to the increase in piezoelectric polarization and spontaneity. Thus, as displayed in Fig. 3, the polarization of AlGaN (piezoelectric and spontaneous) and σ_b increase with hydrostatic pressure. With the increase in hydrostatic pressure, the lattice constants ($a_e(T,P,m), a_0(m)$) increase. Figure 4 shows the dependence of conduction and valance bands on hydrostatic pressure and the location of quantum wells (electrons in the conduction band and holes in the valance band). With increasing pressure, the energy gap increases and the distance between the subbands of quantum wells should also increase. Figure 5 shows an example of a change in an electron quantum well to carefully study the changes in the well and its subbands. Increasing the hydrostatic pressure in the range 0-10 GPa leads to the quantum well depth increase to 75 meV, and the subband energy increase to 20 meV in an absolute magnitude. We need the density of electrons and holes along with the energy of the subbands to study and calculate the absorption coefficient, which was depicted in Figs. 6 and 7 along with the dependence on hydrostatic pressure. According to these shapes, the density of electrons and holes increases with increasing pressure. Figures 6 and 7 demonstrate that the highest density and the highest energy are related to the first subband. Therefore, to calculate the transition energy ($E_{CV}^{1,1}(F)$) and the wave functions in the overlap integral ($M_{cv}(F)$) in the absorption relation, the first band is merely considered by the wave functions and sub-energies. In this transition energy, we also took account of the effect of light and heavy holes in the valance band. Figure 8 shows the valance band energy changes (light and heavy holes in the vicinity of wells). The gamma band is not included in the calculations due to light and heavy holes. According to Fig. 8, the energy difference between light and heavy holes is equal to 9 meV in the vicinity of the hole well. This difference varies with pressure changes (as in the valance band changes in Fig. 3). Another parameter that is important in calculating the absorption coefficient is the hole and electron overlap integral. Figure 9 shows the dependence of the normalized square of overlap integral on the hydrostatic

pressure. As the pressure increases, the separation between the valance and conduction subband energy (^{1,1}) increases so that these variations for light and heavy hole are shown in Fig. 10. As a result, the electron and hole wave functions will have less overlap. The low overlap indicates a decrease in the Coulomb energy of the electron and the hole. It means that the exciton dependence energy decreases with increasing the hydrostatic pressure as shown in the inset of Fig. 10. According to Fig. 11, after determining the pressure dependence of the wave functions, the energy of the subbands and the overlap integral, the absorption coefficient can be calculated from Eq. (27). Moreover, with increasing pressure, the absorbed photon energy increases, and the corresponding wavelength decreases which are related to increasing the bandgaps energy with pressure. In this figure, two peaks are observed for each pressure which are associated with the light and heavy holes of the valance band. According to Fig. 8, light holes have more energy, and therefore will have a shorter wavelength than heavy holes. So small peaks are related to light holes. The second point is associated with changes in the amplitude of the absorption coefficient. As the pressure increases, the amplitude of the absorption coefficient increases. In other words, with increasing pressure, the binding energy of the excitons decreases, as they will have a greater tendency to absorb energy and acquire a stronger binding. The stronger the binding energy, the lower the tendency to absorb energy. Therefore, increasing the pressure will enhance the amplitude.
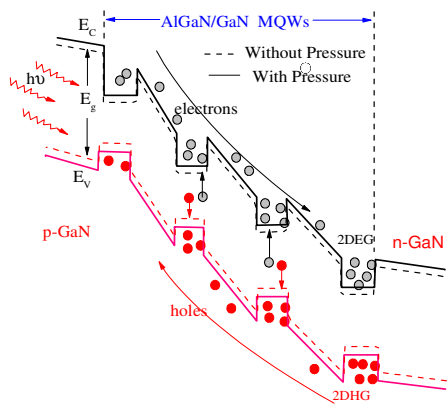

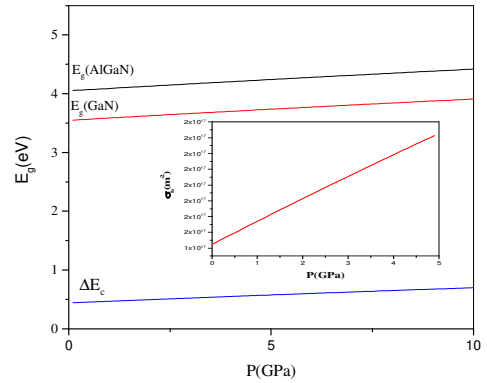Figure 1. Schematic profile of pGaN–i(AlGaN/GaN MQW)–n-GaN.

Figure 2. The band-gaps energy of $Al_{0.3}Ga_{0.3}N$, GaN and conduction band offset of the $Al_{0.3}Ga_{0.3}N/GaN$ as a function of pressure and temperature. The insert indicates the variations in the σ_b versus pressure
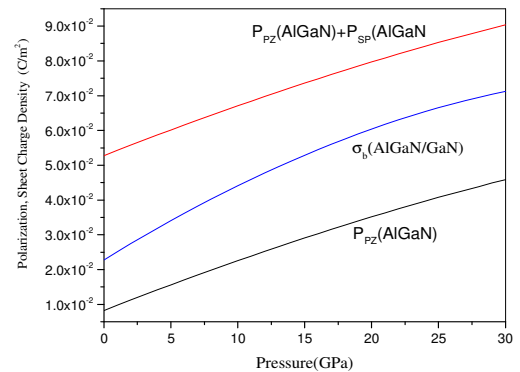

Figure 3. The variation of AlGaN polarization (Piezoelectric and spontaneous) and bound charge at the hetrointerface (σ_b) as a function of the hydrostatic pressure.

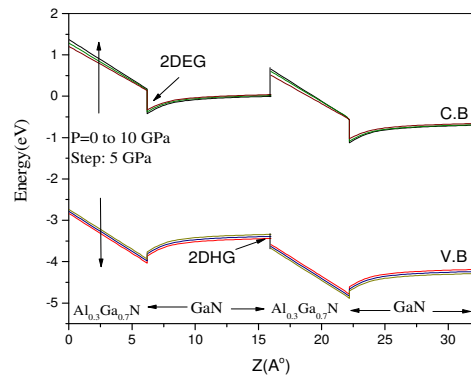Figure 4. The conduction (C.B) and valance (V.B) bands energy of $Al_{0.3}Ga_{0.7}N/GaN/Al_{0.3}Ga_{0.7}N/GaN$ hetrostructure as a function of the distance under different hydrostatic pressure.
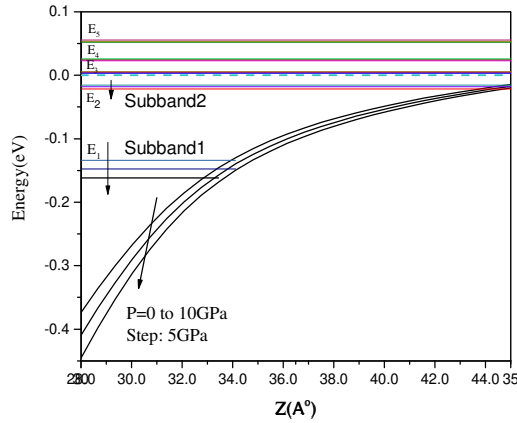
Figure 5. The quantum well conduction band and subband of energy as a function of the distance under different hydrostatic pressure. The insert indicates the variations in the n_{2D} versus pressure.
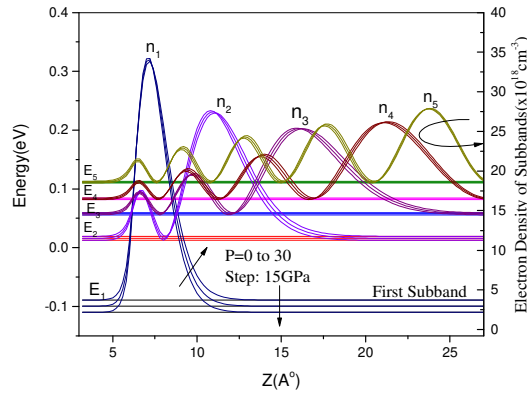

Figure 6. Density of electrons (n_i) along with the energy of the subbands (E_i) of Al$_{0.3}$Ga$_{0.7}$N/GaN hetrostructure versus the distance in different hydrostatic pressure.
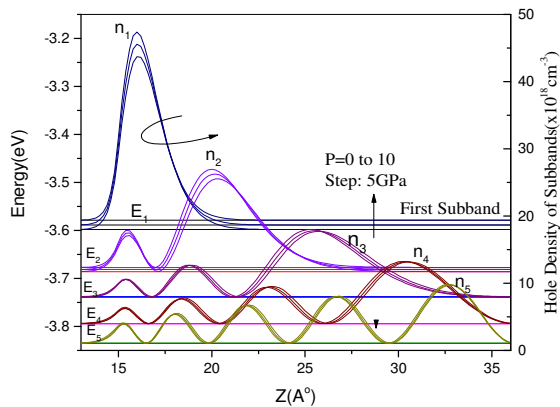

Figure 7. Density of holes (n_i) along with the energy of the subbands (E_i) of Al$_{0.3}$Ga$_{0.7}$N/GaN hetrostructure versus the distance in different hydrostatic pressure.
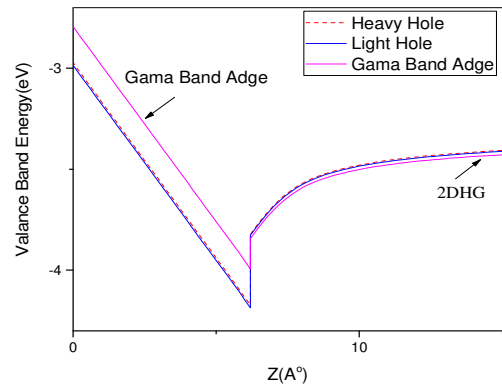

Figure 8. Valance bands energy (Gama, light and heavy holes in the vicinity of 2DHG) versus the distances for Al$_{0.3}$Ga$_{0.7}$N/GaN hetrostructure.

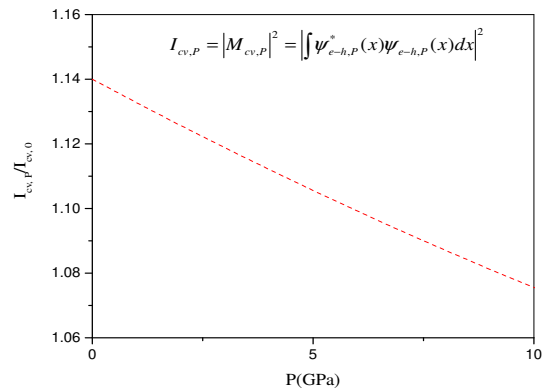$$I_{cv,P} = \left|M_{cv,P}\right|^2 = \left|\int \psi_{e-h,P}^*(x)\psi_{e-h,P}(x)dx\right|^2$$

Figure 9. Normalized square of the overlap of the electron−hole wave functions versus the hydrostatic pressure.
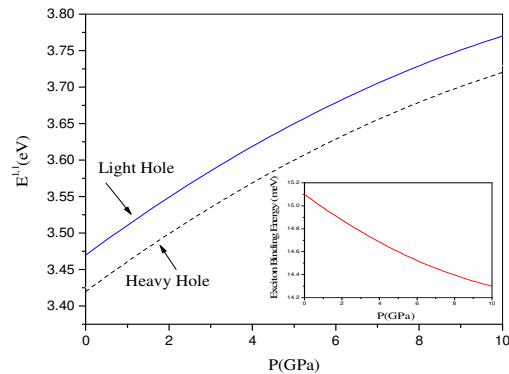

Figure 10. The separation between the valance and conduction subbands $(E_{CV}^{1,1})$ versus the hydrostatic pressure. The insert indicates the exciton binding energy versus pressure.
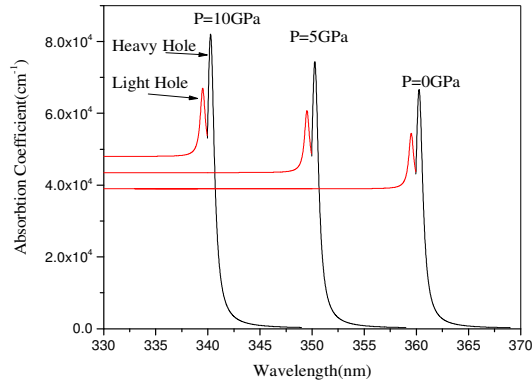
Figure 11. Absorption coefficient for p-GaN–i($Al_{0.3}Ga_{0.7}N$/GaN MQW)–n-GaN versus different hydrostatic pressures.

4 Conclusions

In this study, we examined the optical absorption spectrum of $\mathbf{Al_{0.3}Ga_{0.7}N/GaN}$ multi-quantum well (MQW) under hydrostatic pressure**.** The results showed that the increase in pressure could enhance the polarization charge density $(\boldsymbol{\sigma_b})$. Increasing the hydrostatic pressure in the range of 0-10GPa leads to increasing the conduction band discontinuity from 0.4 to 0.7eV and also increases the distance between the first subband of the conduction band energy and capacity ($E_{CV}^{1,1}$) by 20meV. **At each pressure, the energy difference between light and heavy holes in the valance band is 9meV. Increasing the hydrostatic pressure in the range 0-10 GPa leads to (i), an 8 mV decrease in the exciton bonding energy (corresponding to the first substrates), (II) an increase (height) of the absorption coefficient of 15.8 for heavy holes and 12.8 For light holes, (III) reduces 0.06 overlap of normalized wave functions, and also (IV) reduces the 32 nm of absorption coefficient peaks.**

Acknowledgements

References

[1] R. Chu, "GaN power switches on the rise: Demonstratedbenefits and unrealized potentials.", Applied Physics Letters, **116** (2020) 090502.

[2] G. Hu, L. Lib, Y. Zhang, "Two-dimensional electron gas in piezotronic devices." Nano Energy, **59** (2019) 667.

[3] R. Yahyazadeh, Zahra hashempour, "Effects of Hydrostatic Pressure and Temperature on the AlGaN/GaN High Electron Mobility Transistors. Journal of Interfaces." Thin films and Low dimensional systems, **2** (2019) 183.

[4] R. Yahyazadeh, Z. Hashempour, "Numerical Optimization for Source-Drain Channel Resistance of AlGaN/GaN HEMTS." Journal of Science and technology, **11** (2019) 1.

[5] C. M. Duque, A. L. Morales, M. E. Mora-Ramos, C. A. Duque, "Exciton-related optical properties in zinc-blende GaN/InGaN quantum wells under hydrostatic pressure." Physica Status Solidi (b), **252** (2015) 670.

[6] Z. H. Zhang, J. H. Yuan, K. X. Guo, "The Combined Influence of Hydrostatic Pressure and Temperature on Nonlinear Optical Properties of GaAs/Ga0.7Al0.3As Morse Quantum Well in the Presence of an Applied Magnetic Field." Materials, **11** (2018) 668.

[7] W. Bardyszewski, S. P. Lepkowski, H. Teisseyre, "Pressure Dependence of Exciton Binding Energy in GaN/AlxGa1¡xN Quantum Wells." Acta Physica Polonica A, **119** (2011) 663.

[8] A. Asgari , Kh. Khalili, "Temperature dependence of InGaN/GaN multiple quantum well based high efficiency solar cell." Solar Energy Materials & Solar Cells, **95** (2011) 3124.

[9] P. J. Stevens, M. Whitehea, G. Parry, K. Woobridge, "Computer Modeling of the Electric Field Dependent Absorption Spectrum of Multiple Quantum Well Material." IEEE Journal of Quantum Electronics, **24** (1988) 2007.

[10] Bi. Chouchen, M. H. Gazzah, A. Bajahzar, Hafedh Belmabrouk, "Numerical Modeling of the Electronic and Electrical Characteristics of InGaN/GaN-MQW Solar Cells." Materials, **12** (2019) 1241.

[11] R. Belghouthi, J. P. Salvestrini, M. H. Gazzeh, and C. Chevallier, "Analytical modeling of polarization effects in InGaN double hetero-junction p-i-n solar cells." Superlattices and Microstructures, **100** (2016) 168.

[12] Bi. Chouchen, et al., "Numerical modeling of InGaN/GaN p-i-n solar cells under temperature and hydrostatic pressure effects." AIP Advances, **9** (2019) 045313.

[13] X. Huang, "Piezo-Phototronic Effect in a Quantum Well Structure." ACS Nano, **10** (2016) 5145.

[14] O. Ambacher, A. B Foutz, J Smart, J. R Shealy, N. G Weimann, K Chu, et al., "Two dimensional electron gases induced by spontaneous and piezoelectric polarization in undoped and doped AlGaN/GaN heterostructures." Journal of Applied Physics, **87** (2000) 334.

[15] O. Ambacher, J. Majewski, C. Miskys, et al., "Pyroelectric properties of Al (In) GaN/GaN hetero- and quantum well structures." Journal of Physics Condensed Matter, **14** (2002) 3399.

[16] Z. J. Feng, Z. J. Cheng, and H. Yue, "Temperature dependence of Hall electron density of GaN-based heterostructures." Chinese Physics, **13** (2004) 1334.

[17] V. Fiorentini, F. Bernardini, O. Ambacher. "Evidence for nonlinear macroscopic polarization in III–V nitride alloy Heterostructures." Applied Physics Letters, **80** (2002) 1204.

[18] P. Perlin, L. Mattos, N. A. Shapiro, J. Kruger, W. S. Wong, T. Sands, N. W. Cheung, E. R. Weber, "Reduction of the energy gap pressure coefficient of GaN due to the constraining presence of the sapphire substrate." Journal of Applied Physics, **85** (1999) 2385.

[19] K. J. Bala, A. J. Peter, C. W. Lee, "Simultaneous effects of pressure and temperature on the optical transition energies in a Ga0.7In0.3N/GaN quantum ring." Chemical Physics, **495** (2017) 42.

[20] M. Yang et al., "Effect of polarization coulomb field scattering on parasitic source access resistance and extrinsic transconductance in AlGaN/GaN heterostructure FETs." IEEE Transactions on Electronic Devices, **63** (2016) 1471.

[21] I. Vurgaftman, J. R Meyer, L. R. R Mohan, "Band parameters for III–V compound semiconductors and their alloys." Journal Applied Physics, **89** (2001) 5815.

[22] H. Dakhlaoui, "The effects of doping layer location on the electronic and optical properties of GaN step quantum well." Superlattices and Microstructures, **97** (2016) 439.

[23] P. Perlin, L. Mattos, N. A. Shapiro, J. Kruger, W. S. Wong, T. Sands, N. W. Cheung, E. R. Weber, "Reduction of the energy gap pressure coefficient of GaN due to the constraining presence of the sapphire substrate." Journal Applied Physics, **85** (1999) 2385.

[24] B. Jogai, "Influence of surface states on the two-dimensional electron gas in AlGaN/GaN heterojunction field-effect transistors." Journal of Applied Physics, **93** (2003) 1631.

[25] B. Jogai, "Parasitic Hole Channels in AlGaN/GaN Heterojunction Structures.", physica status solidi b, **233** (2002) 506.